Progress In Electromagnetics Research B, Vol. 73, 17–29, 2017

Analysis of Circular Polarization Backscattering and Target Decomposition Using GB-SAR

Yuta Izumi[1, *], Sevket Demirci[2], Mohd Z. Baharuddin[3], Josaphat T. S. Sumantyo[1], and Heein Yang[1]

Abstract—Currently, most full-polarimetric synthetic aperture radar (SAR) systems adopt linear polarization (LP). On the other hand, circular polarization (CP) is also becoming popular due to its various benefits over LP. However, since CP-SAR is an emerging technique, there are not many imaging and polarimetric analysis results in the literature. As a fundamental study on CP-SAR, this paper presents the results of an investigation on the CP properties of ground-based SAR (GB-SAR) echoes from various canonical targets and a rice paddy sample. The C-band data acquired in a laboratory environment are analyzed and interpreted by means of several factors such as calibration performance, experimental verification of theoretical scattering matrices, imaging quality and accuracy of scattering decomposition results. The eigenvector-based decomposition of the coherency matrix is adopted, and the performance of CP in retrieving the targets' dominant scattering mechanisms and physical parameters is evaluated from entropy-alpha (H-$\bar{\alpha}$) plane and orientation angle ($\bar{\beta}$) value. Results demonstrate the effectiveness of CP in interpreting and discriminating the SAR image features mainly owing to its distinct advantage of highly reliable received signal strength.

1. INTRODUCTION

Conventional synthetic aperture radar (SAR) utilizes linear polarization (LP) where the antenna transmits and receives horizontally (H) and vertically (V) polarized signals. In recent years, various advanced techniques have been developed to aid polarimetric SAR (PolSAR) data interpretation and analysis in LP basis. PolSAR data provides scattering diversity in the form of co-polarization (HH, VV) and cross-polarization (HV, VH) which can be further used for classification purposes. The Japanese ALOS-2, the Canadian RADARSAT-2, and the German TerraSAR-X are recent examples of the state of the art SAR satellites combined with full polarimetric capabilities [1–3].

Currently, the Josaphat Microwave Remote Sensing Laboratory (JMRSL) of Chiba University in Japan is developing SAR systems for unmanned aerial vehicle (UAV), aircraft, and microsatellite platforms using circular polarization (CP), dubbed as CP-SAR [4, 5]. These CP-SAR sensors will be used in several applications such as land cover mapping and disaster monitoring [4]. CP radar has several expected benefits compared to LP radar. Touzi discussed that CP is more effective for ship detection at low off-nadir angle because it can directly detect either odd or even bounce back scattering [6]. CP is also known to be insensitive to Faraday rotation effect, where the reference plane of a transmitted microwave rotates as it propagates through the ionosphere of the Earth. This effect, especially experienced in low frequency L-band LP-SAR satellites causes undesirable reception of the opposing polarization [7, 8]. On the other hand, CP is more resistant to signal degradation due to ionosphere conditions. This advantage results in elimination of polarization mismatch losses [9, 10]. Easier alignment of the antenna on the

Received 17 August 2016, Accepted 8 February 2017, Scheduled 21 February 2017

* Corresponding author: Yuta Izumi (yutaizumi@chiba-u.jp).

[1] Center for Environmental Remote Sensing (CEReS), Chiba University, Japan. [2] Electrical and Electronic Faculty of Engineering, Mersin University, Turkey. [3] Department of Electronics and Communication Engineering, Tenaga National University, Malaysia.

radar platform and the high received signal strength irrespective of the target orientation are the other advantages of CP-SAR systems.

Besides its usefulness, however, CP-SAR is less studied because CP antennas cannot easily meet the design requirements such as gain, bandwidth, and axial ratio (AR). However, it is important to note that the advantages mentioned above usually outweigh this drawback. In [11], Sheen et al. adopted CP antennas for millimeter-wave imaging technique of personal screening to detect the concealed handgun. CP technique has also been utilized in remote sensing of Moon surface by Arecibo telescope to observe a crater on the Moon [12]. In each case, the satellite onboard SAR which transmits and receives CP signal has not been utilized practically for target classification technique such as polarimetric decomposition in Earth observation so far.

This paper presents the polarimetric analysis results of C-band CP-SAR experiments for several canonical targets and a rice paddy sample. The main focus is to experimentally assess the capability of CP-SAR in imaging and polarimetric target decomposition for interpreting scattering mechanisms. To achieve this, we first developed a ground-based (GB) CP-SAR system and conducted stripmap SAR measurements inside an anechoic chamber. To obtain reliable scattering matrices of the targets, a full polarimetric calibration technique which compensates contamination of the radar system was applied to the collected CP-SAR data. For canonical scattering targets, we used a circular plate, a horizontal dihedral, and wires with different orientation angles about line of sight (LOS) which provide single scattering, double bounce scattering, and wire-like (linear) scattering, respectively. To investigate our method on a complex real world target, we performed measurements on rice plants. Among the substantial number of target decomposition techniques, the eigenvector-based decomposition has been exploited to determine the scattering mechanisms and estimate the targets physical parameters.

The paper is organized as follows. The next section introduces various polarimetric parameters in CP basis, the CP formulation of scattering matrix, and the eigenvector-based decomposition. Section 3 provides an explanation of the developed GB CP-SAR system. The experimental results are given in Section 4, followed by an analysis and discussion of the processed data. Last section concludes the paper.

2. POLARIMETRIC THEORY IN CIRCULAR POLARIZATION BASIS

Elliptical polarization (EP) can be generated by simultaneously transmitting H and V polarizations that have a phase shift between each other. Fig. 1 shows the electric field vectors trajectory for a general EP wave. CP is a special case wherein the phase shift between H and V channels is 90°. The rotation direction of a CP signal can be either left handed CP (LHCP: hereafter L) or right handed CP (RHCP: hereafter R), determined by the traveling wave rotation direction observed from a fixed reference plane,

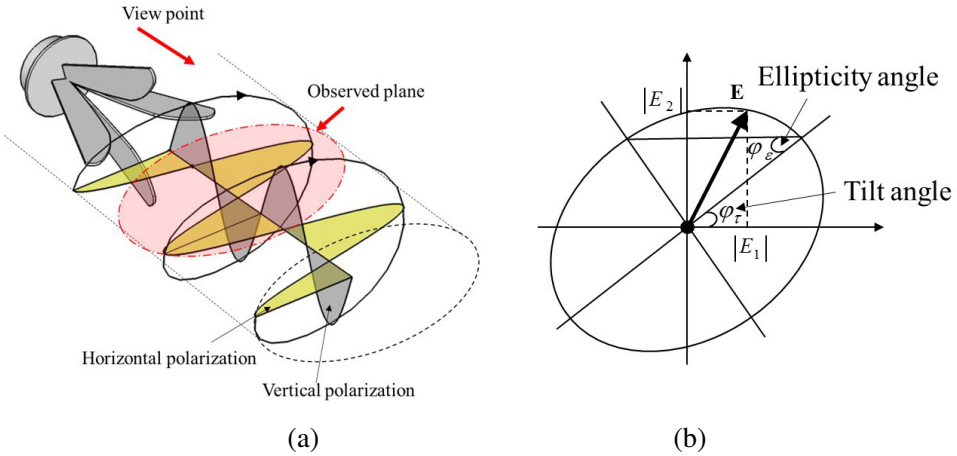

Figure 1. The elliptically polarized wave: (a) Vector trajectory of the elliptically polarized wave. (b) The parameters of the polarization ellipse.

as shown in Fig. 1(a). Fig. 1(b) shows the observation plane's cross-section where φ_ε is the ellipticity angle and φ_τ is the tilt angle [10]. The ovality of ellipse and the sense of rotation are determined by φ_ε and its sign, respectively. The polarization becomes exactly circular when φ_ε is equal to $\pm 45°$. Negative sign of ellipticity angle indicates a right-hand rotation whereas a positive sign is linked to a left hand rotation. On the other hand, polarization is called as linear polarization when φ_ε equals to $0°$.

Polarization state can also be expressed with an AR parameter, which is the ratio of the magnitudes of the fields two orthogonal components and defined in terms of the ellipticity angle φ_ε as [10]:

$$AR = 20\log(\cot(\varphi_\varepsilon)). \tag{1}$$

Theoretically, 0 dB of AR represents an ideal CP whereas an infinite value corresponds to an ideal LP. For CP, however, it is usually difficult to obtain an ideal 0 dB AR over the entire antenna bandwidth, and thus a value of less than 3 dB is considered to be sufficient for most practical cases [13].

2.1. Circular Polarization Scattering Matrix

The scattering matrix in LP basis can be converted to any arbitrary basis by unitary matrix called basis transformation matrix. The basis transformation matrix $[\mathbf{U}_T]$ is defined as [14]

$$[\mathbf{U}_T] = \frac{1}{\sqrt{1+\rho_{\mathrm{LP}}\rho_{\mathrm{LP}}^*}} \begin{bmatrix} 1 & -\rho_{\mathrm{LP}}^* \\ \rho_{\mathrm{LP}}^* & 1 \end{bmatrix} \begin{bmatrix} e^{j\varphi} & 0 \\ 0 & e^{-j\varphi} \end{bmatrix}, \tag{2}$$

where ρ_{LP} is the polarization ratio in LP basis which can be defined by using E_1 and E_2 in Fig. 1(b). ρ_{LP} and φ are calculated by

$$\rho_{\mathrm{LP}} = \frac{E_2}{E_1} = \frac{|E_2|}{|E_1|}e^{j(\phi_2-\phi_1)}, \tag{3}$$

$$\varphi = \tan^{-1}(\tan\varphi_\tau \tan\varphi_\varepsilon), \tag{4}$$

where ϕ_1 and ϕ_2 are the phases of E_1 and E_2, respectively.

As an example, transformation matrix converting from LP to CP basis is obtained by putting values into ρ_{LP} and φ of Eqs. (2), (3), and (4). Ideal CP has $90°$ phase shift and same amplitude between E_1 and E_2, which results in $\rho_{\mathrm{LP}} = j$. Consequently, basis transformation matrix to convert from LP to CP basis with arbitrary tilt angle φ_τ is determined as following:

$$[\mathbf{U}_T]_{\mathrm{CP}} = \frac{1}{\sqrt{2}} \begin{bmatrix} 1 & j \\ j & 1 \end{bmatrix} \begin{bmatrix} e^{j\varphi_\tau} & 0 \\ 0 & e^{-j\varphi_\tau} \end{bmatrix}. \tag{5}$$

The equation to transform scattering matrix in LP basis $[\mathbf{S}]_{\mathrm{LP}}$ to CP basis $[\mathbf{S}]_{\mathrm{CP}}$ with arbitrary tilt angle φ_τ is expressed by:

$$[\mathbf{S}]_{\mathrm{CP}} = [\mathbf{U}_T]_{\mathrm{CP}}^T [\mathbf{S}]_{\mathrm{LP}} [\mathbf{U}_T]_{\mathrm{CP}}, \tag{6}$$

$$\begin{bmatrix} S_{LL} & S_{LR} \\ S_{RL} & S_{RR} \end{bmatrix} = \frac{1}{2} \begin{bmatrix} e^{j\varphi_\tau} & 0 \\ 0 & e^{-j\varphi_\tau} \end{bmatrix} \begin{bmatrix} 1 & j \\ j & 1 \end{bmatrix} \begin{bmatrix} S_{HH} & S_{HV} \\ S_{VH} & S_{VV} \end{bmatrix} \begin{bmatrix} 1 & j \\ j & 1 \end{bmatrix} \begin{bmatrix} e^{j\varphi_\tau} & 0 \\ 0 & e^{-j\varphi_\tau} \end{bmatrix}. \tag{7}$$

2.2. Eigenvector Based Decomposition Theory in CP Basis

Eigenvector based decomposition is a technique that is suited for understanding the physical interpretation of the targets and their randomness, which is based on the statistical matrix such as covariance and coherency matrix [15]. Commonly the coherency matrix was used for this technique since it represents the scattering mechanism. In case of CP basis, the coherency matrix is obtained by converting from LP basis in this study.

The averaged coherency matrix in LP basis is defined using Pauli vector $\mathbf{k}_p$ as:

$$\langle \mathbf{T}_{\mathrm{LP}} \rangle = \frac{1}{n}\sum^{n} \mathbf{k}_p \mathbf{k}_p^\dagger. \tag{8}$$

The coherency matrix in CP basis can be obtained by Pauli vector in CP basis $\mathbf{c}_p$ that is linked to $\mathbf{k}_p$ by using unitary matrix $[\mathbf{U}_c]$, shown as:

$$\mathbf{c}_p = [\mathbf{U}_c]\,\mathbf{k}_p, \tag{9}$$

$$\frac{1}{\sqrt{2}}\begin{bmatrix} S_{LL}+S_{RR} \\ S_{LL}-S_{RR} \\ 2S_{LR} \end{bmatrix} = \frac{1}{\sqrt{2}}\begin{bmatrix} 0 & 0 & j \\ 0 & 1 & 0 \\ j & 0 & 0 \end{bmatrix}\begin{bmatrix} S_{HH}+S_{VV} \\ S_{HH}-S_{VV} \\ 2S_{HV} \end{bmatrix}. \tag{10}$$

Then, coherency matrix in CP basis can be expressed as:

$$\begin{aligned} \langle \mathbf{T}_{\mathrm{CP}} \rangle &= \tfrac{1}{n}\sum^{n} \mathbf{c}_p \mathbf{c}_p^{\dagger} \\ &= \tfrac{1}{n}\sum^{n} [\mathbf{U}_c]\,\mathbf{k}_p \mathbf{k}_p^{\dagger} [\mathbf{U}_c]^{\dagger} \\ &= [\mathbf{U}_c]\,[\mathbf{U}_3]\begin{bmatrix} \lambda_1 & 0 & 0 \\ 0 & \lambda_2 & 0 \\ 0 & 0 & \lambda_3 \end{bmatrix}[\mathbf{U}_3]^{\dagger}[\mathbf{U}_c]^{\dagger} \\ &= [\mathbf{U}]'\begin{bmatrix} \lambda_1 & 0 & 0 \\ 0 & \lambda_2 & 0 \\ 0 & 0 & \lambda_3 \end{bmatrix}[\mathbf{U}]'^{\dagger}, \end{aligned} \tag{11}$$

where λ_i are the eigenvalues, and $[\mathbf{U}_3]$ is unitary orthogonal eigenvector ($\mathbf{u}_i$) matrix which is defined by:

$$[\mathbf{U}_3] = [\ \mathbf{u}_1 \quad \mathbf{u}_2 \quad \mathbf{u}_3\ ] = \begin{bmatrix} \cos\alpha_1 & \cos\alpha_2 & \cos\alpha_3 \\ \sin\alpha_1\cos\beta_1 e^{j\delta_1} & \sin\alpha_2\cos\beta_2 e^{j\delta_2} & \sin\alpha_3\cos\beta_3 e^{j\delta_3} \\ \sin\alpha_1\sin\beta_1 e^{j\gamma_1} & \sin\alpha_2\sin\beta_2 e^{j\gamma_2} & \sin\alpha_3\sin\beta_3 e^{j\gamma_3} \end{bmatrix}. \tag{12}$$

In Eq. (12), phase δ_i expresses the relative phase between $S_{HH}-S_{VV}$ and $S_{HH}+S_{VV}$, similarly phase γ_i is the relative phase between S_{HV} and $S_{HH}+S_{VV}$, α_i is a value that represents intrinsic scattering type, and β_i is related to polarimetric orientation angle about LOS. $[\mathbf{U}]'$ can then be calculated by using $[\mathbf{U}_c]$ of Eq. (10), shown as:

$$[\mathbf{U}]' = [\mathbf{U}_c]\,[\mathbf{U}_3] = \begin{bmatrix} j\sin\alpha_1\sin\beta_1 e^{j\gamma_1} & j\sin\alpha_2\sin\beta_2 e^{j\gamma_2} & j\sin\alpha_3\sin\beta_3 e^{j\gamma_3} \\ \sin\alpha_1\cos\beta_1 e^{j\delta_1} & \sin\alpha_2\cos\beta_2 e^{j\delta_2} & \sin\alpha_3\cos\beta_3 e^{j\delta_3} \\ j\cos\alpha_1 & j\cos\alpha_2 & j\cos\alpha_3 \end{bmatrix}. \tag{13}$$

The decomposition parameters, namely entropy H, averaged alpha angle $\bar{\alpha}$, and averaged beta angle $\bar{\beta}$ are defined as:

$$H = \sum_{i=1}^{3} P_i(-log_3 P_i), \tag{14}$$

$$\bar{\alpha} = \sum_{i=1}^{3} P_i\alpha_i, \tag{15}$$

$$\bar{\beta} = \sum_{i=1}^{3} P_i\beta_i, \tag{16}$$

where

$$P_i = \frac{\lambda_i}{\lambda_1+\lambda_2+\lambda_3}(i=1,2,3). \tag{17}$$

Entropy H is a measure of the randomness of the scattering process where high entropy values indicate the contribution of several scattering mechanisms while lower values imply non-depolarizing single scattering mechanism. Theoretical values of $\bar{\alpha}$ and $\bar{\beta}$ for commonly used canonical targets are listed in Table 1.

Table 1. Theoretical values of alpha and beta angles for various canonical targets.

Target	Averaged alpha angle $\bar{\alpha}$ [°]	Averaged beta angle $\bar{\beta}$ [°]
Plate, Trihedral	0	NA (≈ 0)
Dihedral	90	NA (≈ 0)
Vertical or Horizontal wire	45	NA (≈ 0)
45° inclined wire	45	90

3. GROUND BASED CIRCULARLY POLARIZED SAR SYSTEM

GB CP-SAR system developed in this study consists of a VNA (vector network analyzer), CP horn antennas, an automated positioner controller, and a control PC as depicted in Fig. 2(a). To generate CP signals, a 90° phase shifter with a dual polarized horn antenna was used. Introducing a phase shift

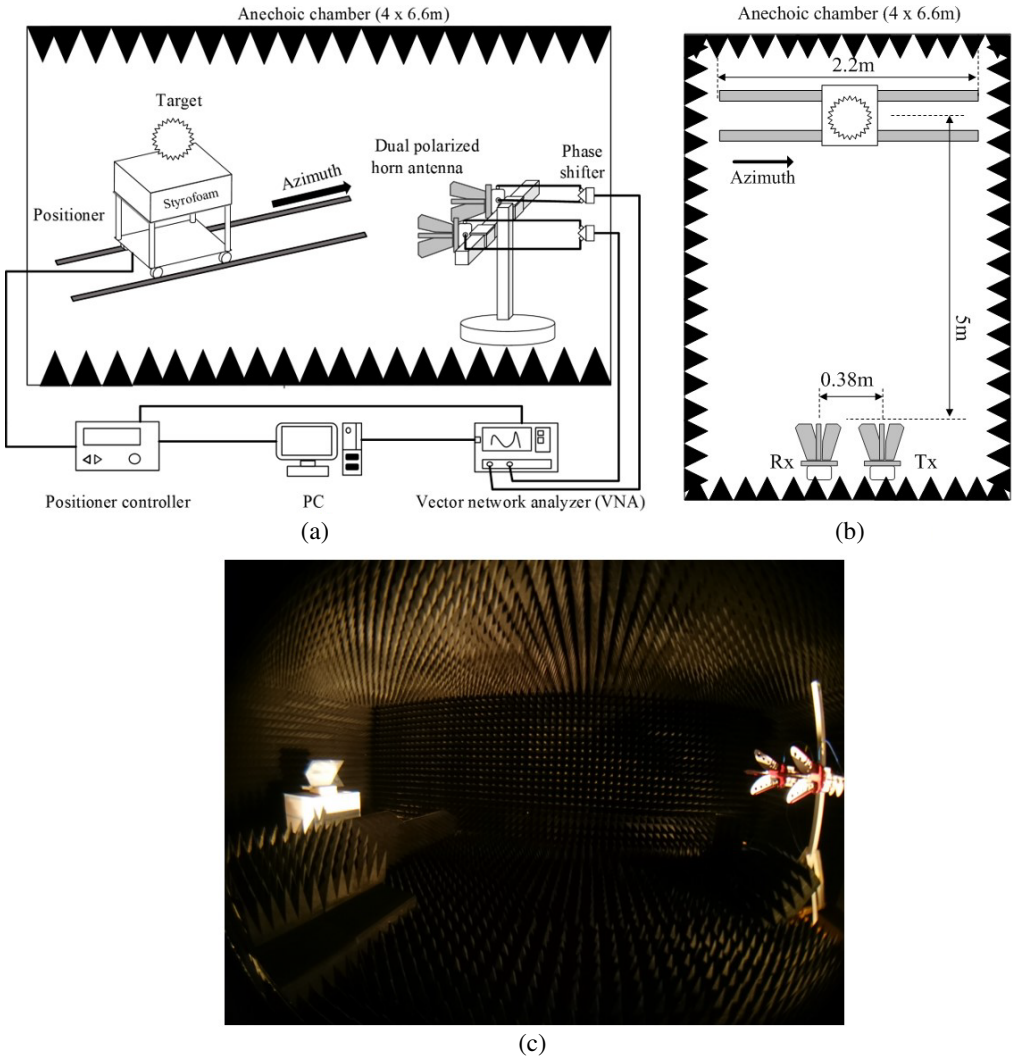

Figure 2. GB CP-SAR system configuration and geometry: (a) SAR system network. (b) Experimental geometry from top view. (c) Photograph from the actual experiment with CP-SAR system and horizontal dihedral target.

into the V-port generates L signal, whereas shifting the H-port phase will generate R signal [16]. The PC triggers and controls both the VNA and positioning mechanism. All parameters such as frequency, output power, frequency sampling points, azimuth sampling points, and the azimuth interval can be set via PC. The experiments within the anechoic chamber were carried out for the C band (4.5 to 7.5 GHz) with 801 frequency sampling points. An automatic positioning device moves the target along a 2.2 meter long rail with 22 mm azimuth interval. Experimental geometry and a sample photograph from the actual experiment are shown in Fig. 2(b) and Fig. 2(c), respectively.

As discussed in the previous section, the AR of an antenna should be less than 3 dB to transmit and receive an approximately ideal CP signal. The AR of the horn antenna used in the experiments was measured by a precise technique inside the anechoic chamber. The obtained results for the operating frequency range is shown in Fig. 3. It is seen that the measured AR is under 2.5 dB except for around 7.2 GHz. According to the definition given in [13], this performance of antenna is found to satisfy the requirements of CP transmission.

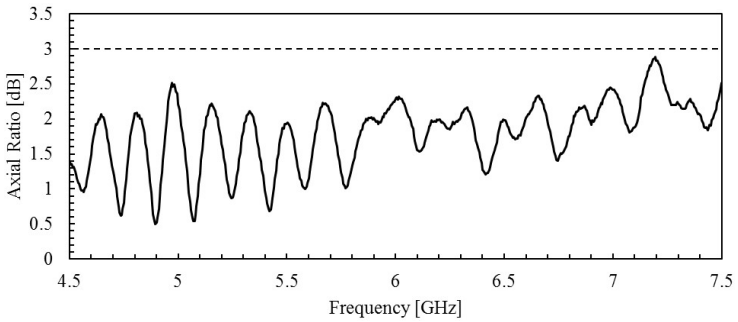

Figure 3. Measured AR graph in range from 4.5 to 7.5 GHz.

3.1. Polarimetric Calibration

Accurate knowledge of the scattering matrices of targets is requisite to obtain highly reliable polarimetric analyses. In practice, however, the measured data is generally contaminated due to the imperfections in the antenna system. To estimate and eliminate this contamination, backscattering measurements of a set of canonical targets with known scattering matrices are generally exploited. Several approaches for LP radars have been developed for this process, called the polarimetric calibration [17–20]. Recently, Izumi et al. proposed a calibration technique for CP radars [21] which is based on the adaptation of Wiesbeck et al.'s LP basis technique [17]. This approach was deployed in this study to calibrate the measured CP-SAR data.

Table 2. Comparison of uncalibrated and calibrated CP scattering matrices of circular plate and vertical dihedral at 6 GHz with respective theoretical scattering matrix.

Target	Theoretical scattering matrix	Uncalibrated scattering matrix	Calibrated scattering matrix
Circular plate	$\begin{bmatrix} 0 & j \\ j & 0 \end{bmatrix}$	$\begin{bmatrix} 0.2062e^{j29.6100^\circ} & 1.0000e^{j0^\circ} \\ 0.956e^{j10.6461^\circ} & 0.1940e^{j132.5669^\circ} \end{bmatrix}$	$\begin{bmatrix} 0.1735e^{j97.2778^\circ} & 0.9875e^{j0.9515^\circ} \\ 1.0000e^{j0^\circ} & 0.1671e^{-j178.2088^\circ} \end{bmatrix}$
Vertical dihedral	$\begin{bmatrix} 1 & 0 \\ 0 & -1 \end{bmatrix}$	$\begin{bmatrix} 0.9684e^{j177.3290^\circ} & 0.1032e^{j9.2996^\circ} \\ 0.0873e^{j3.7739^\circ} & 1.0000e^{j0^\circ} \end{bmatrix}$	$\begin{bmatrix} 1.0000e^{j0^\circ} & 0.0188e^{-j113.3097^\circ} \\ 0.0183e^{-j129.6023^\circ} & 0.9838e^{j178.9414^\circ} \end{bmatrix}$

The calibration targets were selected as a circular plate, a vertical dihedral, and a 45° inclined dihedral. The scatterometric measurements (i.e., static measurements at only one view angle) were performed to estimate the distortion parameters and to remove the errors introduced by these parameters. Using these distortion parameters, calibrated scattering matrices can be calculated. The results for circular plate and vertical dihedral test targets at 6 GHz are shown in Table 2. The comparison of the uncalibrated and calibrated scattering matrices indicates the significant improvements in channel balances of dominant polarizations (S_{LR}/S_{RL} or S_{LL}/S_{RR}). Moreover, the reduction in crosstalk is also clearly seen which validates the effectiveness of calibration.

4. SAR EXPERIMENT IN AN ANECHOIC CHAMBER

To analyze the CP-SAR performance, a GB-SAR experiment was conducted in an anechoic chamber. Focused SAR images were obtained, and then the eigenvector-based decomposition was applied to the target image signatures to estimate the polarimetric scattering parameters H, $\bar{\alpha}$ and $\bar{\beta}$.

The experimental analysis procedure is explained in the following:

(i) Collect CP-SAR data of targets.

(ii) Apply full polarimetric calibration to the collected data.

(iii) Reconstruct CP-SAR images.

(iv) Derive coherency matrices from the focused image data.

(v) Obtain H, $\bar{\alpha}$, and $\bar{\beta}$ values through eigenvector-based decomposition of the coherency matrices.

The CP-SAR images were reconstructed by applying the conventional ω-k algorithm to the collected frequency domain data [22]. The chosen canonical test targets were a circular plate, a horizontal dihedral, a vertical wire, a horizontal wire, and a 45° inclined wire. For a complex target, we measured scattering from rice plants which was set inside a polystyrene foam box with soil and water. The off-nadir angle was set to 90° for canonical targets and 76° for the rice plants. The photographs of the measured targets are seen in Fig. 4.

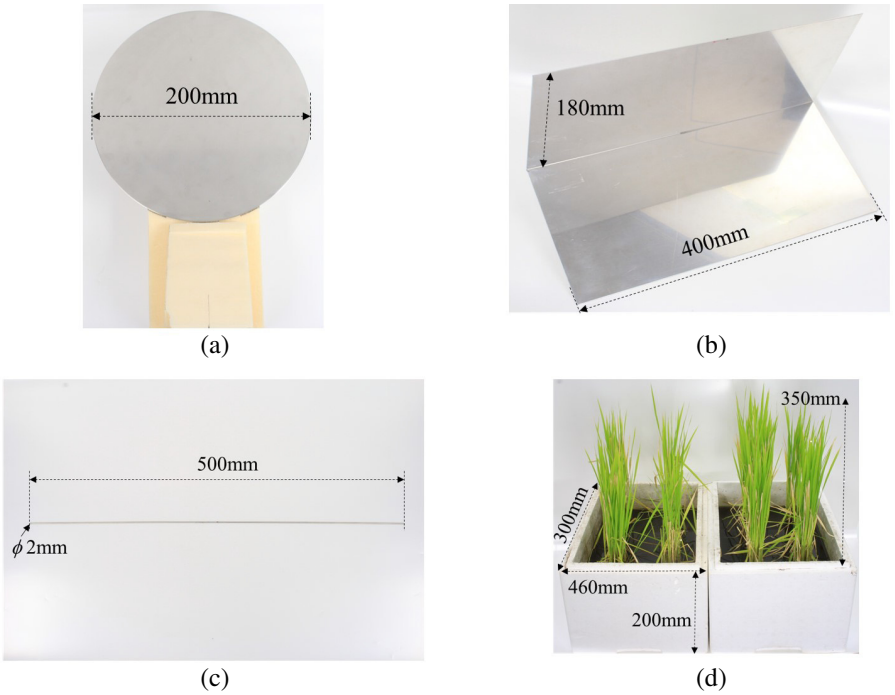

Figure 4. Photographs of the targets used in the experiment: (a) Circular plate. (b) Dihedral. (c) Wire. (d) Rice plants.

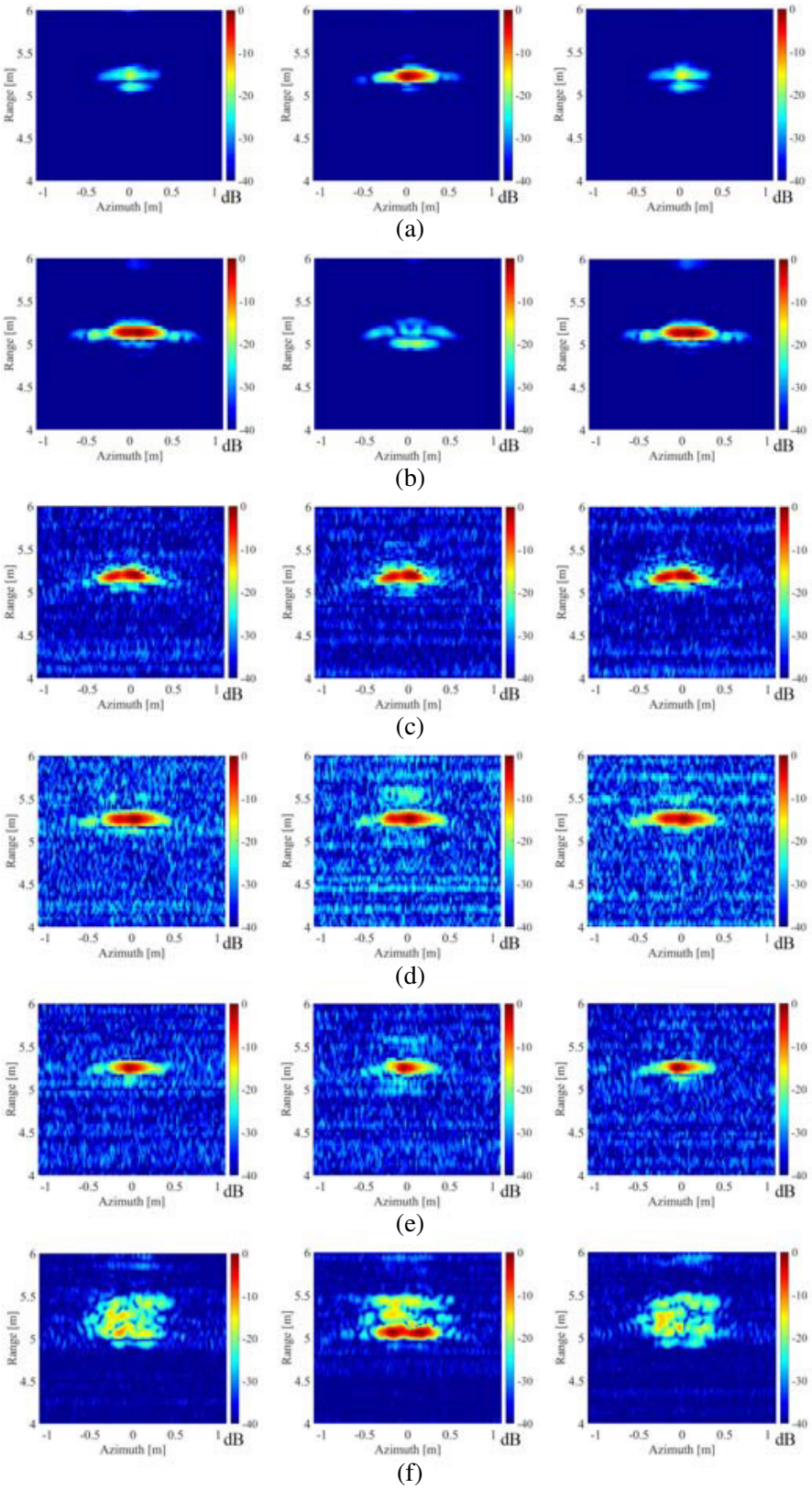

Figure 5. CP-SAR images reconstructed by applying ω-k algorithm (left: LL, middle: LR, right: RR): (a) Circular plate. (b) Horizontal dihedral. (c) Vertical wire. (d) Horizontal wire. (e) 45° inclined wire. (f) Rice plants.

4.1. Experimental Results

Reconstructed CP-SAR images of the targets are shown in Fig. 5 which are displayed on a normalized 40 dB dynamic range. Since S_{RL} images are equal to S_{LR} images under the reciprocity theorem, only the S_{LR} images are included in Fig. 5. These CP-SAR images validate the good imaging ability since the shape of each target was successfully retrieved. Moreover, the wire targets in three orientation angles (i.e., vertical, horizontal, and 45°) exhibit almost same intensity levels for all polarizations, which validates the invariance of CP signal's intensity to LOS rotation of targets. This attribute of CP is usually regarded as important for accurate remote sensing because the effect of Faraday rotation for satellite and antenna misalignment/orientation angle for UAV or aircraft could be reduced by this way.

It is well known that soil and water produce single (surface or specular) scattering, cloud of leafy structures produce volume scattering, and combination of the rice plants with ground surface (dihedral structure) produce double bounce scattering [23]. CP-SAR image provides the knowledge of odd- or even-bounce scattering mechanisms by examining the cross- or co-polarization components respectively. This can be confirmed from the CP-SAR images of the circular plate and the dihedral which are displayed in Fig. 5(a) and Fig. 5(b). However, the detailed analysis is difficult to investigate from only CP-SAR images if wire-like targets exist in the region of interest because scattering mechanism from wire targets contributes to both cross- and co-polarization channels. The CP-SAR images of the rice plants in Fig. 5(f) show single and double bounce scattering mechanisms for LR and LL (or RR) images respectively. However, wire (linear) scattering mechanism is also seen in all polarization images as discussed.

To investigate the phase and amplitude relations between polarimetric channels, the scattering matrices of targets are extracted from the target location (maximum intensity pixel). The scattering matrix of the rice plants is not included since its SAR signatures are not uniform around the target location. The results are shown in Table 3 together with theoretical scattering matrices of each target.

Table 3. Theoretical and measured CP scattering matrices of canonical targets.

Target	Theoretical scattering matrix	Measured scattering matrix
Circular plate	$\begin{bmatrix} 0 & j \\ j & 0 \end{bmatrix}$	$\begin{bmatrix} 0.1451e^{-j170.4987^\circ} & 0.9493e^{-j17.1594^\circ} \\ 1.0000e^{j0^\circ} & 0.1866e^{-j16.2642^\circ} \end{bmatrix}$
Horizontal dihedral	$\begin{bmatrix} 1 & 0 \\ 0 & -1 \end{bmatrix}$	$\begin{bmatrix} 1.0000e^{j0^\circ} & 0.1293e^{-j40.6913^\circ} \\ 0.1244e^{-j53.5900^\circ} & 0.9954e^{j176.1457^\circ} \end{bmatrix}$
Vertical wire	$\frac{1}{2}\begin{bmatrix} 1 & j \\ j & -1 \end{bmatrix}$	$\begin{bmatrix} 0.9665e^{j172.3562^\circ} & 0.9225e^{j93.2553^\circ} \\ 0.9762e^{j97.1914^\circ} & 1.0000e^{j0^\circ} \end{bmatrix}$
Horizontal wire	$\frac{1}{2}\begin{bmatrix} -1 & j \\ j & 1 \end{bmatrix}$	$\begin{bmatrix} 1.0000e^{j0^\circ} & 0.9995e^{j86.6877^\circ} \\ 0.8612e^{j93.2656^\circ} & 0.9659e^{j170.2806^\circ} \end{bmatrix}$
45° inclined wire	$\frac{1}{2}\begin{bmatrix} j & j \\ j & j \end{bmatrix}$	$\begin{bmatrix} 0.9125e^{j3.7878^\circ} & 0.8350e^{j22.9336^\circ} \\ 0.8206e^{j7.1116^\circ} & 1.0000e^{j0^\circ} \end{bmatrix}$

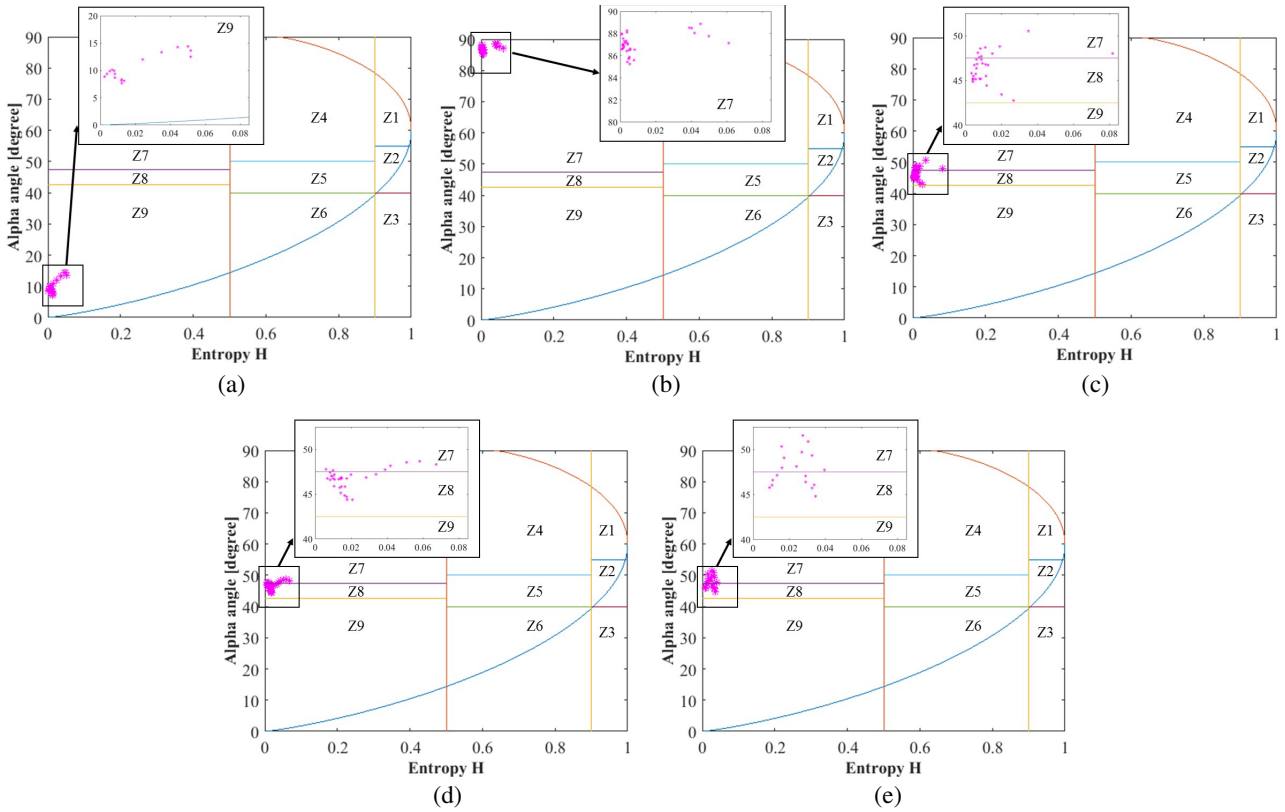

Figure 6. H-$\bar{\alpha}$ distribution (target location pixels): (a) Circular plate. (b) Horizontal dihedral. (c) Vertical wire. (d) Horizontal wire. (e) 45° inclined wire.

Table 4. Measured $\bar{\beta}$ values of canonical targets averaged over the target location pixels.

Target	Averaged $\bar{\beta}$ [°]
Circular plate	16.9202
Horizontal dihedral	2.3037
Vertical wire	6.6481
Horizontal wire	4.5553
45° inclined wire	80.8578

The relative phases and amplitudes are seen to be in good agreement with their correct values owing to the effective polarimetric calibration.

The eigenvector-based decomposition is then applied to LL, LR, and RR image data set. These polarization data are converted to coherency matrix and also averaged by moving average filter (3×3 window size). The H and $\bar{\alpha}$ results for the deployed canonical targets are displayed on the H-$\bar{\alpha}$ plane, as shown in Fig. 6 (only target pixels are considered). The $\bar{\beta}$ values are acquired by averaging over the target region which are listed in Table 4. For the rice plants, H, $\bar{\alpha}$, and $\bar{\beta}$ images are generated and displayed in Fig. 7.

H-$\bar{\alpha}$ plane is commonly used for unsupervised classification with some special zones which indicate different scattering mechanisms [15]. Since our canonical targets are regarded as point-target circular plate, dihedral, and wire, they should lie in the regions of; low entropy surface scattering ($Z9$ in Fig. 6),

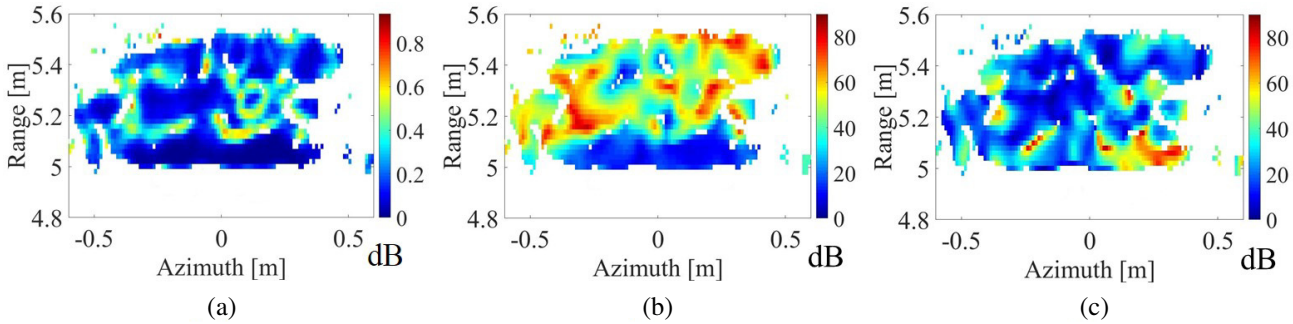

Figure 7. H, $\bar{\alpha}$, and $\bar{\beta}$ images of the rice plants (only the target location): (a) H image, (b) $\bar{\alpha}$ image, (c) $\bar{\beta}$ image.

multiple (even-bounce) scattering ($Z7$ in Fig. 6) and wire-like scattering ($Z8$ in Fig. 6), respectively [15]. The results from Fig. 6 demonstrate that all canonical targets are observed to be within the true zones. The $\bar{\alpha}$ of the circular plate and the dihedral show the values in consistent with theory listed in Table 1. The wire targets in three orientations exhibit similar H-$\bar{\alpha}$ distributions for all orientations and $\bar{\alpha}$ of all cases are consistent with theory (45°) either. From Table 4, the $\bar{\beta}$ of the circular plate shows $\approx 17°$ error value relative to theoretical one (0°) that implies the necessity of more accurate alignment of targets and/or calibration. The dihedral, horizontal wire, and vertical wire show similar value ($\approx 0°$) while the 45° inclined wire indicates $\approx 81°$ of $\bar{\beta}$ which is close to theoretical $\bar{\beta}$ value (90°).

The H image of the rice plants in Fig. 7 shows high entropy value (≈ 0.6) in some areas. These high entropy areas can be observed in around planted area, indicating multiple scattering mechanisms. The $\bar{\alpha}$ image of the rice plants exhibits $\approx 0°$, $\approx 45°$, and $\approx 90°$ values which implies surface, wire-like (linear), and double bounce scattering mechanism respectively. The $\bar{\beta}$ image of the rice plants displays $\approx 0°$ value except for some small areas which verifies that no inclined scatters are existing. Overall, although each rice cannot be recognized due to low resolution, the brief contribution of each scattering mechanism could be displayed by this decomposition technique in CP-basis.

5. CONCLUSIONS

In this research, the CP-SAR capability is investigated in terms of imaging and polarimetric decomposition performance through CP-SAR imaging experiments conducted in an anechoic chamber. We developed a GB CP-SAR system that comprised of a VNA, horn antennas with 90° phase shifters, automated positioning system, and PC, which can be operated within C-band. To precisely evaluate the CP-SAR performance, a polarimetric calibration technique for CP-radar was employed. Several canonical and complex targets; namely a circular plate, a horizontal dihedral, a vertical wire, a horizontal wire, a 45° inclined wire, and rice plants were selected for the imaging targets.

The obtained CP-SAR images were able to capture the forms of each target and have scattering matrices in satisfactory agreement with theoretical ones. The wire targets in three orientations (vertical, horizontal, and 45°) produced similar intensity levels among all polarizations which experimentally proves that the invariance of CP signal's intensity to LOS rotation of targets. The eigenvector-based decomposition parameters H, $\bar{\alpha}$, and $\bar{\beta}$ that were derived from CP-SAR images were also in close agreement with theory. The $\bar{\beta}$ of the 45° inclined wire target showed $\approx 90°$ while other targets showed $\approx 0°$. Moreover, the rice plants showed brief classification result within the planted area. From the experimental results, we confirmed that the less intensity effect of orientation angle in CP-SAR image and unsupervised classification capability using polarimetric decomposition technique.

This research contributes to the ground-based validation study about CP-SAR polarimetry which leads to the JMRSL next generation mission of CP-SAR for UAV, aircraft, and microsatellite. Further analysis will be implemented in outdoor experiment as a ground-based observation and after the CP-SAR mission starts operation in the near future.

ACKNOWLEDGMENT

This work was supported in part by the Japan Science and Technology Agency (JST) — Japan International Cooperation Agency (JICA) FY2010-2016 Science and Technology Research Partnership for Sustainable Development (SATREPS); the European Space Agency (ESA) Earth Observation Category 1 under Grant 6613; the 4th Japan Aerospace Exploration Agency (JAXA) ALOS Research Announcement under Grant 1024; the 6th JAXA ALOS Research Announcement under Grant 3170; the Japanese Government National Budget — Ministry of Education and Technology (MEXT) FY2015-2017 under Grant 2101; Chiba University Strategic Priority Research Promotion Program FY2016-FY2018; Taiwan National Space Organization (NSPO); and Indonesian National Institute of Aeronautics and Space (LAPAN).

REFERENCES

1. Kankaku, Y., Y. Osawa, S. Suzuki, and T. Watanabe, "The overview of the L band SAR onboard ALOS-2," *PIERS Proceedings*, 735–738, Moscow, Russia, August 18–21, 2009.
2. Morena, C. L., K. V. James, and J. Beck, "An introduction to the RADARSAT-2 mission," *Canadian Journal of Remote Sensing*, Vol. 30, No. 3, 221–234, 2004.
3. Werninghaus, R. and S. Buckreuss, "The TerraSAR-X mission and system design," *in IEEE Transactions on Geoscience and Remote Sensing*, Vol. 48, No. 2, 606–614, 2010.
4. Sri Sumantyo, J. T. and N. Imura, "Development of circularly polarized synthetic aperture radar for aircraft and microsatellite," *IEEE Geoscience and Remote Sensing Symposium*, Beijing, China, 2016.
5. Akbar, P. R., J. T. Sri Sumantyo, and H. Kuze, "A novel circularly polarized synthetic aperture radar (CP-SAR) system onboard a spaceborne platform," *International Journal of Remote Sensing*, Vol. 31, No. 4, 1053–1060, 2009.
6. Touzi, R. and C. Franois, "Requirements on the calibration of hybrid-compact SAR," *IEEE Geoscience and Remote Sensing Symposium*, 1109–1112, Quebec City, QC, July 2014.
7. Freeman, A., "Calibration of linearly polarized polarimetric SAR data subject to Faraday rotation," *IEEE Transactions on Geoscience and Remote Sensing*, Vol. 42, No. 8, 1617–1624, 2004.
8. Wright, P. A., S. Quegan, N. S. Wheadon, and C. D. Hall, "Faraday rotation effects on L band spaceborne SAR data," *IEEE Transactions on Geoscience and Remote Sensing*, Vol. 41, No. 12, 2735–2744, 2003.
9. ITU, *Handbook on Satellite Communication*, Wiley, New York, 2002.
10. Warren, L. S., *Polarization in Electromagnetic Systems*, Artech house, Boston, 1993.
11. Sheen, D. M., D. L. McMakin, W. M. Lechelt, and J. W. Griffin, "Circularly polarized millimeter-wave imaging for personnel screening," *Proceedings of the SPIE — International Society for Optical Engineering*, 117–126, Florida, USA, 2005.
12. Campbell, B. A., "Planetary geology with imaging radar: Insights from earth-based lunar studies," *Publications of the Astronomical Society of the Pacific*, Vol. 128, No. 964, 2001–2015, 2016.
13. Gao, S., Q. Luo, and F. Zhu, *Circularly Polarized Antennas*, John Wiley and Sons, West Sussex, 2013.
14. Yamaguchi, Y., *Radar Polarimetry from Basics to Applications: Radar Remote Sensing Using Polarimetric Information*, IEICE, Tokyo, 2007.
15. Cloude, S. R. and E. Pottier, "An entropy based classification scheme for land applications of polarimetric SAR," *in IEEE Transactions on Geoscience and Remote Sensing*, Vol. 35, No. 1, 68–78, 1997.
16. Raney, R. K., "Hybrid-polarity SAR architecture," *in IEEE Transactions on Geoscience and Remote Sensing*, Vol. 45, No. 11, 3397–3404, 2007.
17. Wiesbeck, W. and D. Kahny, "Single reference, three target calibration and error correction for monostatic, polarimetric free space measurements," *in Proceedings of the IEEE*, Vol. 79, No. 10, 1551–1558, 1991.

18. Yueh, S. H., J. A. Kong, R. M. Barnes, and R. T. Shin, "Calibration of polarimetric radars using in-scene reflectors," *Journal of Electromagnetic Waves and Applications*, Vol. 4, No. 1, 27–48, 2012.
19. Gau, J. R. and W. D. Burnside, "New polarimetric calibration technique using a single calibration dihedral," *in IEE Proceedings — Microwaves, Antennas and Propagation*, Vol. 142, No. 1, 19–25, 1995.
20. Chen, T. J., T. H. Chu, and F. C. Chen, "A new calibration algorithm of wide-band polarimetric measurement system," *in IEEE Transactions on Antennas and Propagation*, Vol. 39, No. 8, 1188–1192, 1991.
21. Izumi, Y., S. Demirci, M. Z. Baharuddin, and J. T. Sri Sumantyo, "The polarimetric calibration method for ground-based circularly polarized synthetic aperture radar," *PIERS Proceedings*, 5131–5135, Shanghai, China, August 8–11, 2016.
22. Mehrdad, S., *Synthetic Aperture Radar Signal Processing with MATLAB Algorithms*, Wiley, New York, 1999.
23. Wang, C., J. Wu, Y. Zhang, G. Pan, J. Qi, and W. A. Salas, "Characterizing L-band scattering of paddy rice in Southeast China with radiative transfer model and multitemporal ALOS/PALSAR imagery," *in IEEE Transactions on Geoscience and Remote Sensing*, Vol. 47, No. 4, 988–998, 2009.